Enhanced cadmium removal from water by hydroxyapatite subjected to different thermal treatments

R. Aouay, S. Jebri, A. Rebelo, J. M. F. Ferreira and I. Khattech

ABSTRACT

Hydroxyapatite powders were synthesized according to a wet precipitation route and then subjected to heat treatments within the temperature range of 200–800 °C. The prepared samples were tested as sorbents for cadmium in an aqueous medium. The best performances were obtained with the material treated at 200 °C (HAp_{200}), as the relevant sorbent textural features (S_{BET} – specific surface area and V_p – total volume of pores) were least affected at this low calcination temperature. The maximum adsorption capacity at standard ambient temperature and pressure was 216.6 mg g^{-1}, which increased to 240.7 mg g^{-1} by increasing the temperature from 25 to 40 °C, suggesting an endothermic nature of the adsorption process. Moreover, these data indicated that a thermal treatment at 200 °C enhanced the ability of the material in Cd^{2+} uptake by more than 100% compared to other similar studies. The adsorption kinetic process was better described by the pseudo-second-order kinetic model. Langmuir, Freundlich, and Dubinin–Kaganer–Radushkevich isotherms were applied to describe the sorption behaviour of Cd^{2+} ions onto the best adsorbent. Furthermore, a thermodynamic study was also performed to determine $\Delta H°$, $\Delta S°$, and $\Delta G°$ of the sorption process of this adsorbent. The adsorption mechanisms were investigated by Fourier transform infrared spectroscopy (FTIR) and scanning electron microscopy-transmission electron microscopy (SEM-TEM) observations.

Key words | Cd^{2+} adsorption, heat treatment, hydroxyapatite, isotherms, thermodynamic study

R. Aouay (corresponding author)
I. Khattech
Materials Cristal Chemistry and Applied Thermodynamics Laboratory, Chemistry Department,
LR015SE01, Université de Tunis El Manar, Faculty of Science,
Tunis 2092,
Tunisia
E-mail: *rachida.aouay@fst.utm.tn*

S. Jebri
Natural Water Treatment Laboratory, Water Researches and Technologies Center,
Technologic Park of Borj Cedria,
B.P. 273, Soliman 8020,
Tunisia

A. Rebelo
J. M. F. Ferreira
Department of Materials and Ceramics Engineering, CICECO-Aveiro Institute of Materials,
University of Aveiro,
3810-193 Aveiro,
Portugal

HIGHLIGHTS

- The powder calcined at 200 °C (HAp_{200}) exhibited the maximum Cd^{2+} uptake capacity.
- Relevant sorbent features (S_{BET} and V_p) were least affected for the powder calcined at 200 °C.
- Maximum adsorption capacity at standard ambient temperature and pressure was 216 mg g^{-1}.
- Uptake capacity was improved by more than 100% compared to other studies.

doi: 10.2166/aqua.2020.069

GRAPHICAL ABSTRACT

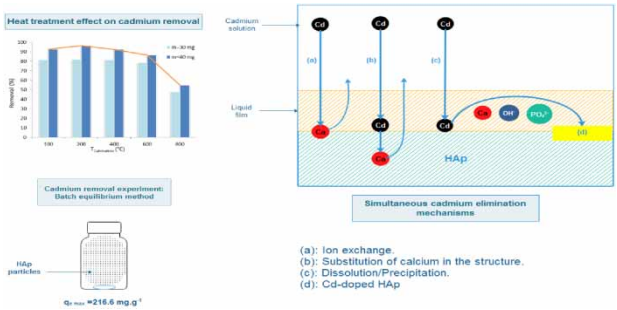

INTRODUCTION

Heavy metals are generally introduced to the environment through discharged domestic, industrial, and agricultural wastewater. Released into the water system, these effluents are of potential threat to surface and ground waters. One of the most hazardous pollutants among the various contaminants that have been added to groundwater is cadmium (Idrees *et al.* 2018). Its presence in drinking water has been considered as a major public health threat. Indeed, chronic exposure to cadmium results in kidney dysfunction (Johri *et al.* 2010), bone, and cardiovascular diseases (Yingjian *et al.* 2017). Moreover, epidemiological studies showed a link between inhalation exposure and the development of lung and prostate cancer (Chen *et al.* 2016). When released into the water systems, these effluents constitute potential threats to the aquatic organisms and public health, as they can accumulate and be transferred up the food chain, threatening food safety and posing serious health risks (Rajeshkumar & Li 2018). Therefore, great attention to the removal of Cd from wastewater is required before it reaches the environmental water sources. In this way, several physicochemical treatments have been applied to reduce this metal in water systems, such as chemical precipitation (Matusik *et al.* 2008), ion exchange (Wong *et al.* 2014), membrane filtration (Kheriji *et al.* 2015), and adsorption process (Harja *et al.* 2015; Naeem *et al.* 2019). Among these remediation techniques, the adsorption procedure has the advantage of being highly efficient, economical, and a simple handling method.

Apatites are a large class of mineral compounds with the general chemical formula $M_{10}(PO_4)_6X_2$, where M is mostly a divalent cation (Ca^{2+}, Sr^{2+}, Ba^{2+}, Cd^{2+}, Pb^{2+}, etc.) and X is a monovalent or bivalent anion (F^-, Cl^-, Br^-, OH^-, CO_3^{2-}) (Elliot 1994). The ability of these materials to exchange several ions in both of the cationic and anionic sites makes them highly effective sorbents for Cd(II) and other trace metals from contaminated soils and wastewaters (He *et al.* 2013). Among apatites, hydroxyapatite with the chemical formula $Ca_{10}(PO_4)_6(OH)_2$ (HAp) is the main mineral component of the calcified tissues (bone and teeth). The crystallinity, the porosity, and the surface characteristics of HAp are correlated to the synthesis and heat treatment conditions. Hence, the sorption behaviour of HAp is highly affected by either morphology or the crystalline state (Stötzel *et al.* 2009; Wang *et al.* 2016).

It was reported that the sorption capacity of the as-prepared HAp sample with the S_{BET} value of 94.9 $m^2\,g^{-1}$ was 142.8 mg of Cd^{2+} per gram of adsorbent (Mobasherpour *et al.* 2011). On the other hand, this quantity was reduced to 70.9 and 16.9 mg of Cd^{2+} per gram of adsorbent by the effect of calcination at temperatures ranging from 500 to 1,140 °C (Da Rocha *et al.* 2002). However, no study has been conducted for powders calcined at low and moderate temperatures. Therefore, the purpose of this work is to investigate the dependence of the Cd^{2+} removal efficiency of HAp powders on the calcination temperature and to determine the best heat treatment conditions that allow

maximizing it. Moreover, the adsorption process dynamics was studied as a function of pH, adsorbent dosage, contact time, initial metal concentration, and temperature, and the adsorption isotherms were established.

MATERIALS AND METHODS

Materials preparation

HAp powders were synthesized by wet chemical precipitation (Jebri *et al.* 2017). The method involves a dropwise addition of a diammonium hydrogen phosphate solution $(NH_4)_2HPO_4$ (0.31 M) into a boiling solution of calcium nitrate $Ca(NO_3)_2{\cdot}4H_2O$ (0.12 M) at normal pressure. The pH of precipitation medium has been maintained close to 11 by successive additions of ammonia solution (28 wt%). The precipitate was separated by vacuum filtration. The filtrate was washed by distilled water and dried for 12 h at 100 °C. Finally, the as-obtained powders were calcined at various temperatures for 12 h. The synthesis can be schematized by the following reaction:

$$10Ca(NO_3)_2 + 6(NH_4)_2HPO_4 + 8NH_4OH \rightarrow Ca_{10}(PO_4)_6(OH)_2 + 20NH_4NO_3 + 6H_2O$$

All the reactants used in the experiments are of analytical grade and manufactured by Merck and Fluka.

Sorption procedure

The study of Cd^{2+} sorption onto HAp was carried out through the batch equilibrium technique. The influence of adsorbent calcination temperature on the Cd^{2+} removal was investigated. The effects of used adsorbent amount, the contact time, the pH, the initial metal concentration, and the solution temperature were also studied.

For these purposes, aqueous solutions of Cd^{2+} ions with various concentrations were prepared by diluting a stock solution containing 2.7445 g of $Cd(NO_3)_2{\cdot}4H_2O$ per litre of distilled water.

The adsorption studies were carried out by mixing 10–60 mg of adsorbent with 100 mL of Cd^{2+} solutions at various concentrations. Furthermore, the acidity/alkalinity of the medium was varied from pH ~2 up to weakly basic conditions (pH ~8) by dropwise adding of 0.1 M aqueous solutions of HCl or KOH to study the effect of pH variation. To assure the accomplishment of adsorption equilibrium, the suspension was stirred for 120 min (Mobasherpour *et al.* 2011) at 300 rpm and then sampled through vacuum filtration for further analysis of the remaining adsorbate. The amount of the adsorbed Cd^{2+} per gram of adsorbent q_t (mg g^{-1}) at time t is calculated as follows:

$$q_t = \frac{(C_0 - C_t)}{m} V \quad (1)$$

where C_0 and C_t are the metal ion concentrations (mg L^{-1}) in the liquid phase initially and at any time t, respectively, m is the mass of the adsorbent (g), and V is the volume of the solution (L). After 120 min, C_t and q_t reach the equilibrium value C_e and q_e.

Analytical methods

The HAp precipitate was subjected to calcination temperatures in the range of 200–800 °C with a heating rate of 20 °C min^{-1} using a Nabertherm Muffle Furnace. X-ray diffraction analysis (XRD) was conducted with a D8 ADVANCE Bruker diffractometer using copper radiations ($K_{\alpha1} = 1.5406$ Å; $K_{\alpha2} = 1.5445$ Å). Data were collected from 10 to 80° 2θ using the step scanning technique. A refinement of the structure using PANalytical X'Pert HighScore Plus V3.0.5 software, allowed determination of the lattice parameters and the crystallite size. According to Landi *et al.* (2000), the fraction of the crystalline phase x_c could be evaluated using the following relation:

$$x_c \approx 1 - \left(\frac{V_{112/300}}{I_{300}}\right) \quad (2)$$

where I_{300} is the intensity of the (300) reflection and $V_{112/300}$ is the intensity of the hollow between (112) and (300) reflections which completely disappears in non-crystalline samples.

Fourier transform infrared spectroscopy (FTIR) was carried out on pellets prepared by mixing 1 mg of the

sample with 200 mg of infrared grade KBr. The spectra were recorded between 400 and 4,000 cm^{-1} using the IRAffinity-1 Shimadzu spectrophotometer. Nitrogen adsorption–desorption isotherms were performed with a Micromeritics ASAP 2020 at 77 K. The S_{BET} of the particles was calculated using the Brunauer–Emmett–Teller (BET) method in the range of relative pressure (p/p_0) from 0.01 to 0.99. The average pore diameter was evaluated by the Barrett–Joyner–Halenda (BJH) method applied to the desorption branch. The morphological features of the material before and after contact with Cd^{2+} solutions were determined using an Ultra-high-Resolution Analytical Electron Microscope (HR-FESEM Hitachi SU-70) and a Transmission Electron Microscope (Hitachi, H9000 NAR). In the liquid phase, the changes in concentrations of Cd^{2+} ions resulting from the interactions with the sorbent were measured by atomic absorption spectrometer type novAA® 350 Analytik Jena.

RESULTS AND DISCUSSION

Characterization of HAp powders

XRD patterns of the apatitic precipitate (100 °C) and those of HAp samples heat-treated at temperatures in the range of 200–800 °C are shown in Figure 1(a). The results indicate

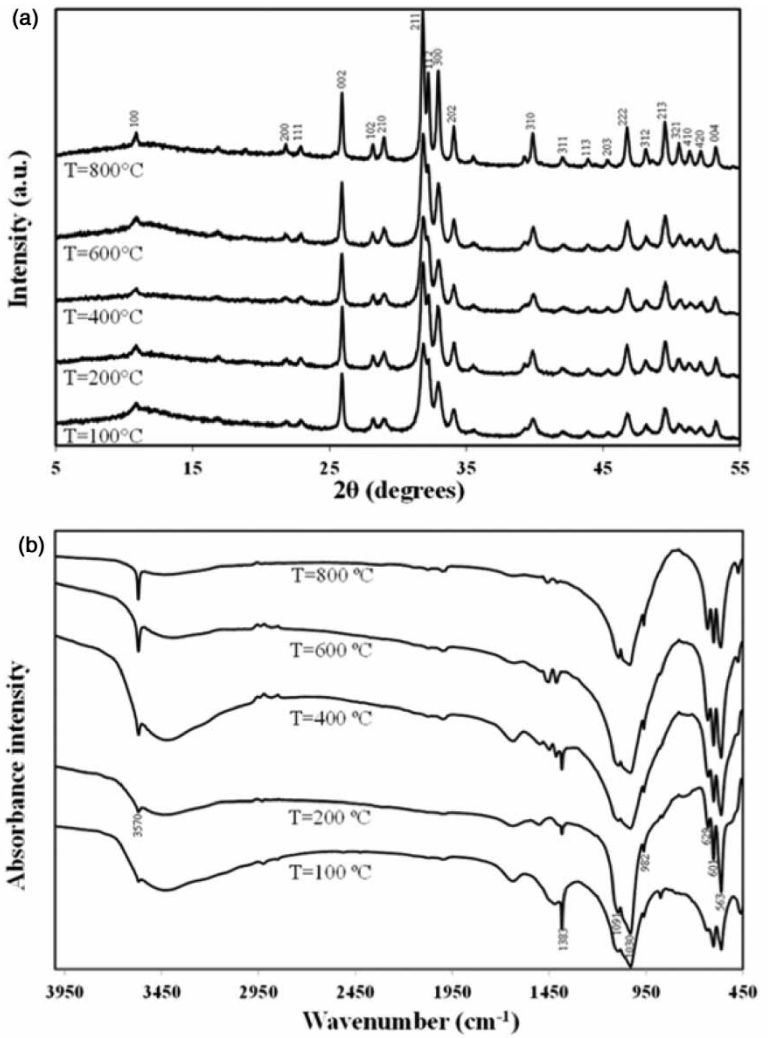

Figure 1 | XRD patterns (a) and infrared spectra (b) of hydroxyapatite powders calcined at different temperatures.

the presence of the crystalline apatitic phase even in the dried powder. The intensity of the XRD peaks was progressively enhanced by increasing the calcination temperature. This evolution is mainly reflected by the increase in the hollow between (112) and (300) reflections on the recorded diagram. Based on the Landi method (Landi *et al.* 2000), the estimated crystalline phase x_c are 0.50, 0.55, 0.60, 0.70, and 0.85 for the products heated at 100, 200, 400, 600, and 800, respectively.

The lattice parameters determined for the highly crystallized sample heat-treated at 800 °C ($x_c = 0.85$) are $a = b =$ 9.417 Å, $c = 6.880$ Å, whereas the crystallite sizes vary within the range 30–40 nm according to the heating temperature. The FTIR spectra of the samples displayed in Figure 1(b) exhibit the characteristic absorbance bands of OH^- groups centred at 629 and 3,570 cm^{-1}, and of PO_4^{3-} groups appearing at 563, 601, 982, 1,030, and 1,091 cm^{-1}. The intensities of these bands increase with increasing the heat treatment temperature, while the absorption band located at 1,383 cm^{-1}, relative to nitrate ions adsorbed on the apatite surface during the synthesis, progressively disappears.

In order to elucidate the effect of calcination temperature on the surface properties of HAp, the powders heated at the extreme temperatures were subjected to the physisorption of N_2. The results plotted in Figure 2 show that the samples are predominantly mesoporous, as evidenced by the type IV isotherms. However, the material heated at 200 °C exhibits a higher hysteresis loop (at $p/p_0 > 0.9$) compared to that treated at 800 °C ($0.12 < p/p_0 < 0.96$). The data collected in Table 1 show significant decreases of pore diameter (D_p) and total pore volume (V_p) for the HAp_{200} powder. Similarly, the surface area (S_{BET}) has been reduced by more than five times by the heat treatment at 800 °C. C_{BET} measures the adsorption force of the first adsorbed nitrogen layer. Consequently, this parameter is directly related to the affinity of nitrogen toward the material surface (Jelinek & Kováts 1994). The decrease of C_{BET} value indicates the low affinity of nitrogen toward the surface of the sample calcined at 800 °C.

Table 1 | Textural features of HAp samples heated at 200 and 800 °C

Sample	S_{BET} ($m^2\,g^{-1}$)	V_p ($cm^2\,g^{-1}$)	D_p (Å)	C_{BET}
HAp_{200}	58.1	0.237	327	123.1
HAp_{800}	10.8	0.014	159	97.4

Optimization of the sorption parameters

Effect of the heat treatment

To study the heat treatment impact of HAp over its Cd^{2+} removal efficiency, masses of 30 and 40 mg of powders calcined at predefined temperatures were equilibrated with the metal ion solution at an initial concentration of 10 mg L^{-1} Cd^{2+}. These experiments were conducted for initial solutions under slightly acidic (pH = 5.2) and under neutral conditions (pH = 7). For both masses, the results are illustrated in Figure 3(a) and 3(b). It can be seen that the highest Cd^{2+} removal percentages were observed for the material heated at 200 °C. Indeed, such treatment allowed releasing the residues of the synthesis inserted into the pores of the apatite, explaining the slight increase in Cd^{2+} uptake compared to the dried raw material. These results were predictable by FTIR analyses that indicated a

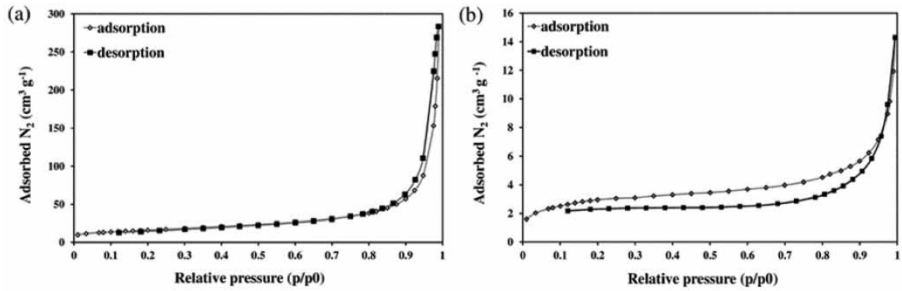

Figure 2 | Nitrogen adsorption–desorption isotherms for hydroxyapatite treated at 200 °C (a) and 800 °C (b).

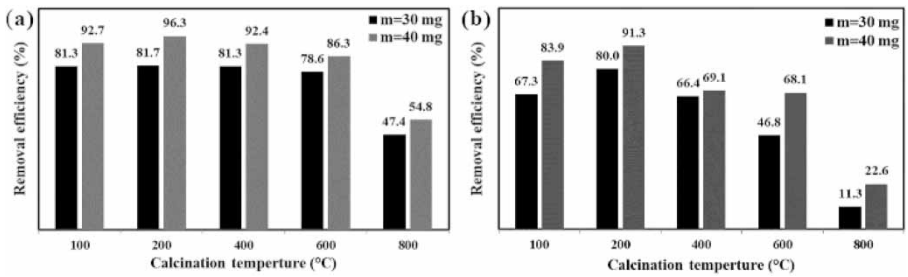

Figure 3 | Evolution of Cd^{2+} removal by adsorption onto HAp powders heated at various temperatures (a) at pH = 5.2 (b) at pH = 7 (Conditions: $[Cd^{2+}]_0 = 10$ mg L^{-1}, $V = 100$ mL, $m = 30$ and 40 mg, $t = 120$ min).

significant decrease of the absorbance band of nitrate between 100 and 200 °C. On the other hand, the adsorption efficiency is considerably reduced by heating the material to 800 °C. This decrease in the adsorption ability can be explained by the reduction of the textural features of the material. Indeed, according to the results of BET analyses reported in Table 1, the rise of the calcination temperature induced concomitant decreases in S_{BET} and V_p. Such trends are in accordance with scanning electron microscopy (SEM) results illustrated in Figure 11, HAp_{200}'s surface is more heterogeneous than that of HAp_{800}.

Based on these results, the optimization of the other parameters on the adsorption of Cd^{2+} onto Hap powder has been carried out with the material heat-treated at 200 °C, denoted as HAp_{200}.

Effect of the initial pH

The results of Cd^{2+} removal efficiency exerted by 40 mg HAp_{200} adsorbent dispersed in 10 mg L^{-1} of Cd^{2+} solution are plotted in Figure 4. These results reveal that the initial solution pH does not play any significant role, except for the extreme values. The slight decrease in the removal percentage observed below pH 3 could be attributed to a partial dissolution of HAp and the competition between H_3O^+ protons and Cd^{2+} ions for the same adsorption surface sites. Accordingly, no adsorption tests were conducted below pH = 2 to prevent the dissolution of apatite in the acid medium. The upper slight alkaline pH limit was selected to avoid the precipitation of Cd-hydroxide forms in an alkaline medium. However, the observed small apparent decrease suggests that under these conditions, some Cd^{2+} ions started reacting with

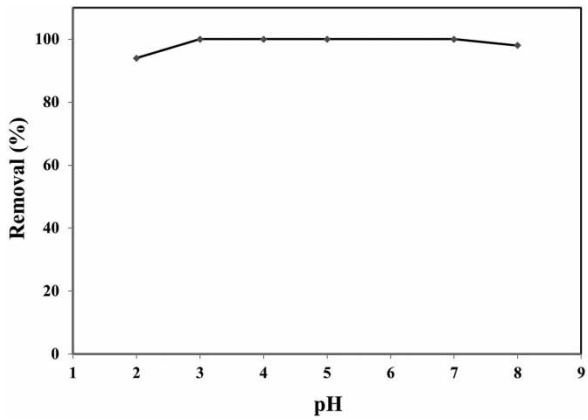

Figure 4 | Effect of the pH on the removal of Cd^{2+} by HAp_{200} (Conditions: $[Cd^{2+}]_0 = 10$ mg L^{-1}, $V = 100$ mL, $m = 40$ mg, $t = 120$ min).

OH^-. As a result, the optimal performance of HAp_{200} is obtained in the pH range of 3–7. It has been shown that the reactions responsible for the surface properties of HAp in aqueous systems are $\equiv PO^- + H^+ \leftrightarrow \equiv P-OH^0$ and $\equiv Ca(OH)_2^+ \leftrightarrow \equiv Ca(OH)^0 + H^+$. In the pH range lower than 6, the predominate reactive sites on the surface of HAp are $\equiv P-OH^0$ and $\equiv Ca(OH)_2^+$. So, the sorption of Cd^{2+} occurs by ion-exchange between H^+ on the surface sites and the metal ion according to the following reactions:

$$\equiv P-OH^0 + Cd^{2+}_{aq} \leftrightarrow \equiv P-O-Cd^+ + H^+_{aq};$$

$$2 \equiv P-OH^0 + Cd^{2+}_{aq} \leftrightarrow (\equiv P-O)_2Cd + 2H^+_{aq}$$

Under alkaline conditions, the surface becomes negatively charged and the predominate species are $\equiv PO^-$ and $\equiv Ca(OH)^0$. In this case, the uptake of Cd^{2+} is governed by the electrostatic forces.

Effect of the adsorbent dose

The effect of the adsorbent amount on Cd^{2+} removal by HAp_{200} is depicted in Figure 5. It can be seen that the removal efficiency increases (although at a decreasing pace) with increasing the amounts of HAp_{200} up to an optimum dosage of 0.4 g L^{-1}, beyond which it becomes approximately constant. The observed trend can be understood considering the insufficient surface area available at the beginning of the experience, forcing the saturation of the active surface sites. However, with increasing adsorbent doses, higher amounts of active surface sites become available for adsorption, and the equilibrium between the Cd^{2+} concentrations at the surface and in the solution is accomplished for gradually lower degrees of adsorbent surface saturation.

Effect of the contact time

The removal percentages of Cd^{2+} ions as a function of the contact time for initial metal concentrations of 10, 50, and 100 mg L^{-1} are reported in Figure 6. It could be noticed that the highest adsorption of metal ions is observed in the first half-hour of contact. This phenomenon could be explained by the availability of a high number of active sites at the beginning of the adsorption process, which gradually decreases as time progresses. Furthermore, the required period for the establishment of equilibrium extraction decreases to 15 min by increasing the initial metal concentration to 100 mg L^{-1}. These results are very consistent, demonstrating that the increasing initial Cd^{2+} concentrations drive the equilibrium toward the surface saturation, exhausting the active surface sites and hindering the further removal capacity of the adsorbent (Adebowale *et al.* 2006). This explains the clear decreasing trends in the removal capacity with increasing concentrations of metal ions. Accordingly, under the tested experimental conditions, the uptake capacities were 25.0, 123.6, and 216.6 mg g^{-1} for initial Cd^{2+} concentrations of 10, 50, and 100 mg L^{-1}, respectively.

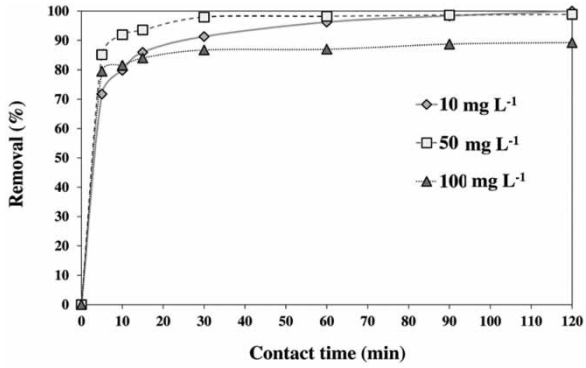

Figure 6 | Contact time effect on Cd^{2+} sorption onto HAp_{200} (Conditions: $[Cd^{2+}]_0 = 10$, 50, and 100 mg L^{-1}, $V = 100$ mL, $m = 40$ mg).

Effect of the solution temperature

Figure 7 shows the evolution of the uptake capacity at different temperatures (298, 303, 308, and 313 K) for an initial metal concentration of 100 mg L^{-1}. It can be seen that the adsorption capacity of the apatite increased from ~217 to

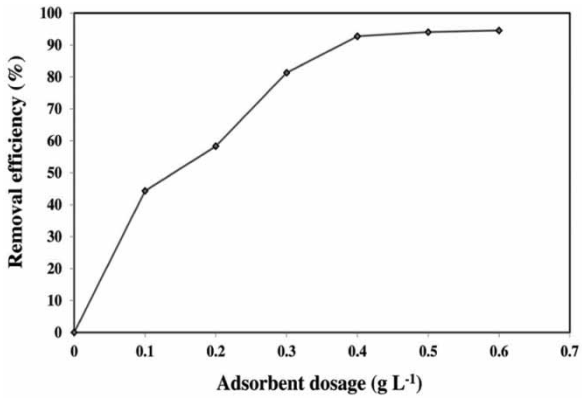

Figure 5 | Effect of adsorbent dosage on Cd^{2+} removal (Conditions: $[Cd^{2+}]_0 = 10$ mg L^{-1}, $V = 100$ mL, pH = 5.2, $t = 120$ min).

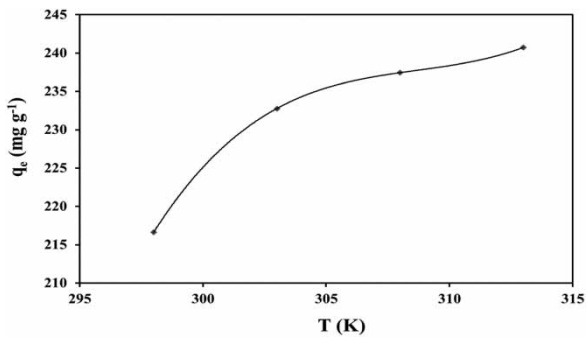

Figure 7 | Effect of the solution temperature on the uptake of Cd^{2+} ions by HAp_{200} (Conditions: $[Cd^{2+}]_0 = 100$ mg L^{-1}, $V = 100$ mL, $m = 40$ mg, $t = 120$ min).

~241 mg g^{-1} with the rise of the temperature, suggesting an endothermic nature of the adsorption process. The increase in the adsorption rate of Cd^{2+} ions can be explained by an increase in the mobility of the metal ions with the rise of the temperature, which favours their interaction with the active sites on the surface of HAp_{200}. Furthermore, the increasing temperature may produce a swelling effect within the internal structure of the adsorbent, enabling large metal ions to cross the external boundary layer and the internal pores (Dogan & Alkan 2003).

Sorption kinetics study

To predict the mechanism involved in the adsorption process of Cd^{2+} ions onto HAp_{200}, several kinetic models have been applied to fit the experimental results. The models are the pseudo-first-order, the pseudo-second-order, Elovich, and the intraparticle diffusion kinetic models.

The linearized form of the pseudo-first-order and the pseudo-second-order kinetic models can be described by the following equations (Lagergren 1898; Ho 2006):

$$\ln(q_e - q_t) = \ln\ q_e - k_1 t \tag{3}$$

$$\frac{t}{q_t} = \frac{1}{k_2 q_e^2} + \frac{1}{q_e} t \tag{4}$$

In Equations (3) and (4), q_e and q_t are the amounts of the sorbed adsorbate at the equilibrium extraction and at the contact time t, respectively (both in mg g^{-1}). The k_1 and k_2 are the pseudo-first-order and pseudo-second-order sorption constants in (min^{-1}) and g (mg $min)^{-1}$, respectively. They are determined through the linear plots of $\ln(q_e–q_t)$ and t/q_t versus t (Figure 8(a) and 8(b)), the gathered data are presented in Table 2. It can be noticed that the correlation coefficients R^2 values obtained for the pseudo-second-order kinetic model are much higher than those found by applying the pseudo-first-order kinetic model. Besides, the experimental amounts of the adsorbed metal ($q_{e,exp}$) are very close to those deduced from the pseudo-second-order kinetic model ($q_{e,cal}$). Thus, the adsorption process can be

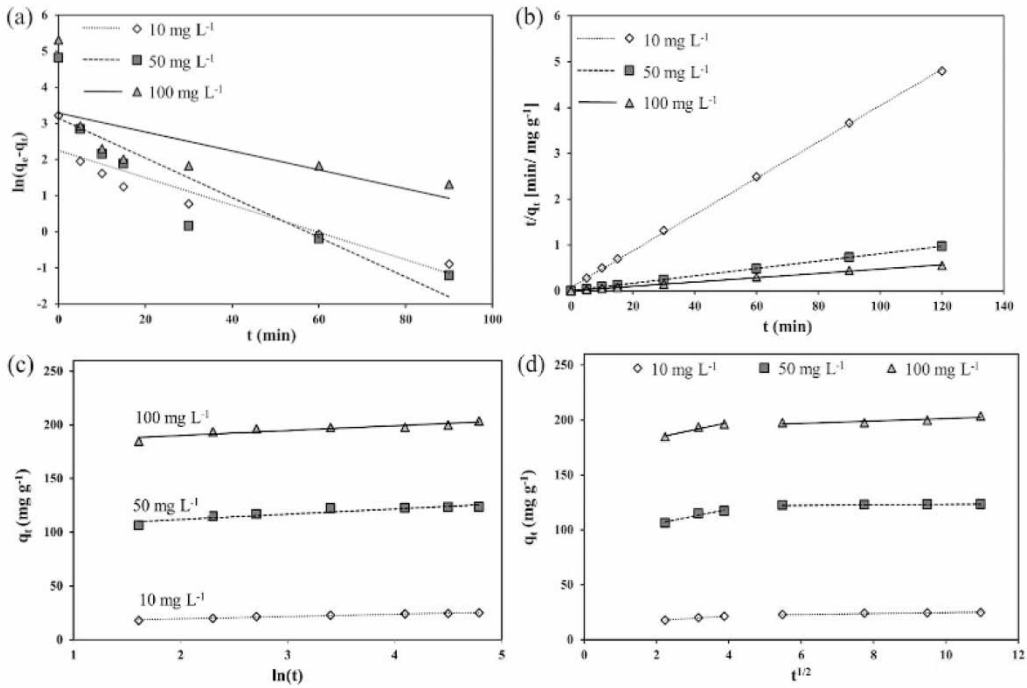

Figure 8 | Experimental data fitting for adsorption of Cd^{2+} ions onto HAp_{200} according to the pseudo-first-order (a), pseudo-second-order (b), Elovich (c), and intraparticle diffusion kinetic models (d).

well described by the pseudo-second-order kinetics model. This result shows that the rate-limiting step could be chemisorption involving valency forces though the sharing of electrons between the active sites of adsorbent and adsorbate as covalent forces and ion-exchange (Ho 2006). A similarity was observed for other previous studies devoted on the kinetics of heavy metals adsorption onto phosphate materials (Elkady *et al.* 2011). Considering the pseudo-second-order constant k_2, the initial adsorption rate h [mg (g min)$^{-1}$] can be expressed as $h = k_2 q_e^2$. The calculated data are reported in Table 2.

The applicability of the Elovich model to sorption kinetics was investigated using the linearized form given by the following equation (Chien & Clayton 1980):

$$q_t = \frac{1}{\beta} \ln (\alpha\beta) + \frac{1}{\beta} \ln (t) \quad (5)$$

where α is the initial adsorption rate and β is a constant related to the extent of surface coverage and activation energy for chemisorption reactions, in mg (g min)$^{-1}$ and (g mg^{-1}), respectively. These parameters could be estimated from the slope and the intercept of the straight-line plot of q_t versus ln t (Figure 8(c)). The calculated parameters are listed in Table 2. They are obtained with a quite high correlation coefficient ($0.8378 \leq R^2 \leq 0.9729$). The increase of the initial adsorption rate constant α with the initial metal concentration supports the chemisorption occurrence during the adsorption process.

The possibility of intraparticle diffusion was also explored. The adsorbate species could be transported from the bulk of the solution into the solid phase through the intraparticle diffusion-transport process, which is often the rate-limiting step especially in a rapidly stirred batch reactor (Weber & Chakravoti 1974). The diffusion model is expressed as follows (Weber & Morris 1963):

$$q_t = k_{id} t^{1/2} + I \quad (6)$$

in which, k_{id} is the intraparticle diffusion rate [mg (g min$^{1/2}$)$^{-1}$]. Values of I give an idea about the boundary layer thickness. In fact, the larger I, the greater is the boundary layer effect (McKay *et al.* 1985). The adsorption capacity q_t was reported as a function of the square root of time $t^{1/2}$ for different initial Cd^{2+} concentrations (Figure 8(d)). The curves exhibit two separate regions attributed to the film diffusion followed by the intraparticle diffusion. Indeed, the first linear portion covers the time range between 5 and 15 min and corresponds to external metal ion diffusion and binding by active sites distributed on the outer surface of the adsorbent. The second lasts from 30 to 120 min, assigned to the establishment of the equilibrium. For each initial metal concentration, values of $k_{id,1}$, $k_{id,2}$ and I_1, I_2 are determined from the slopes and the intercepts of the two straight lines, respectively. The results are gathered in Table 2. It is clear to see that the thickness of the boundary layers in the second portion related to the intraparticle diffusion (I_2) is larger than that of the first portion, which is relative to the film diffusion (I_1). Thus, and accordingly, the film diffusion rate, $k_{id,1}$, is far greater than the

Table 2 | Kinetic parameters for adsorption of Cd^{2+} ions onto HAp_{200} at 298 K

	$[Cd^{2+}]_0$ (mg L^{-1})		
	10	**50**	**100**
$q_{e,exp}$ (mg g^{-1})	25.0	123.6	216.6
Pseudo-first-order model			
$q_{e,cal}$ (mg g^{-1})	9.6	23.2	27.0
k_1 (min^{-1})	0.038	0.055	0.026
R^2	0.8729	0.7905	0.4304
Pseudo-second-order model			
$q_{e,cal}$ (mg g^{-1})	25.2	123.5	204.1
k_2 [g (mg min)$^{-1}$]	0.019	0.014	0.008
h [mg (g min)$^{-1}$]	11.9	208.3	344.8
R^2	0.9994	1	0.9998
Elovich model			
α [mg (g min)$^{-1}$]	2.2×10^4	4.6×10^{10}	1.2×10^{18}
β (g mg^{-1})	0.460	0.202	0.221
R^2	0.9729	0.8526	0.8378
Intraparticle diffusion model			
$k_{id,1}$ (mg (g min$^{0.5}$)$^{-1}$)	2.18	6.59	7.00
I_1	13.1	92.5	170.0
R^2	1	0.931	0.946
$k_{id,2}$ [mg (g min$^{0.5}$)$^{-1}$]	0.39	0.22	1.11
I_2	20.8	121.2	190.3
R^2	0.9704	0.9825	0.7877

intraparticle diffusion rate $k_{id,2}$. Moreover, the linear portions of the curves did not pass through the origin. Therefore, intraparticle diffusion was not the rate-limiting step and the removal of Cd^{2+} ions by Hap_{200} involves some other processes that may be operating simultaneously.

Adsorption isotherms

The equilibrium adsorption studies were performed to evaluate the maximum adsorption capacity of the adsorbent toward the adsorbate and to predict the type of interactions between them. Thus, several equations for isotherms have been proposed. However, Langmuir, Freundlich, and Dubinin–Kaganer–Radushkevich (DKR) models are the most appropriate for equilibrium modelling of heavy metals adsorption onto calcium phosphates.

Langmuir model assumes monolayer adsorption of the adsorbate onto a finite number of identical sites of the adsorbent surface and there is no interaction between the adsorbed species. Mathematically, this model is expressed by the following equation:

$$\frac{C_e}{q_e} = \frac{1}{bq_m} + \left(\frac{1}{q_m}\right) C_e \tag{7}$$

in which, C_e is the equilibrium concentration of the metal ions (mg L^{-1}), q_e is the equilibrium sorption capacity (mg g^{-1}), q_m is the maximum sorption capacity (mg g^{-1}), and b is the Langmuir constant related to the energy of adsorption (L mg^{-1}).

Freundlich isotherm was also applied to study the distribution of Cd^{2+} ions between the liquid and the solid phases. According to this model, the adsorption occurs on a heterogeneous surface through a multilayer adsorption mechanism. Freundlich equation can be written as follows:

$$\ln(q_e) = \ln(k_f) + \left(\frac{1}{n}\right) \ln(C_e) \tag{8}$$

in which, k_f is the Freundlich isotherm constant and n is an empirical parameter related to the intensity of the adsorption which varies with the adsorbent heterogeneity. Thus, if $(1/n)$ values are in the range of 0.1–1, the adsorption conditions are favourable.

The DKR model has been successfully applied to describe the sorption of Cd^{2+} ions onto HAp. The DKR equation can be written as follows:

$$\ln(C_{ads}) = \ln(X_m) - \beta\varepsilon^2 \tag{9}$$

where C_{ads} is the number of metal ions adsorbed per unit mass of adsorbent (mol g^{-1}), X_m is the maximum sorption capacity determined through this model (mol g^{-1}), β is the activity coefficient related to mean sorption energy ($mol^2\ J^{-2}$), and ϵ is the Polanyi potential which is expressed as:

$$\varepsilon = RT \ln(1 + 1/C_e) \tag{10}$$

Accordingly, the sorption potential is a temperature-dependent parameter, specific to the nature of sorbent and sorbate (Dada *et al.* 2012). The slope of the plot of $\ln(C_{ads})$ versus ϵ^2 gives β and the intercept yields the sorption capacity X_m. The sorption space in the vicinity of a solid surface is characterized by a series of equipotential surfaces having the same sorption potential. The sorption energy E could be estimated through the following equation:

$$E = \frac{1}{\sqrt{-2\beta}} \tag{11}$$

The magnitude of apparent energy E is useful to estimate the type of adsorption. So, E value below 8 kJ mol^{-1} indicates physical adsorption. Between 8 and 16 kJ mol^{-1}, the adsorption process can be described by ion exchange, and over 16 kJ mol^{-1}, it is governed by stronger chemical adsorption rather than by ion exchange (Lin & Juang 2002).

In this study, the equilibrium data for Cd(II) distribution between the solid and the liquid phases at 298 K are determined by varying the initial metal concentration from 10 to 100 mg L^{-1}. The adsorption isotherm of Cd^{2+} on HAp_{200} is depicted in Figure 9(a). This latter was correlated according to Langmuir, Freundlich, and DKR models (Figure 9(b)–9(d)).

The sorption constants determined from the selected three models together with their corresponding correlation coefficients are gathered in Table 3. It can be noticed that

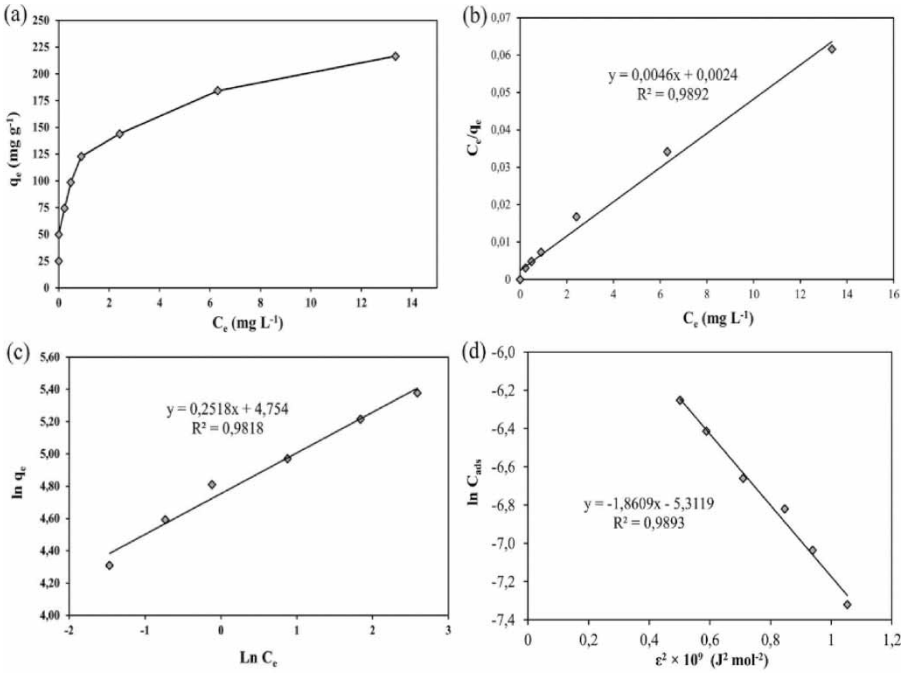

Figure 9 | Isotherm of Cd^{2+} sorption onto HAp_{200} at 298 K (a) and linear fits of experimental data according to Langmuir (b), Freundlich (c), and DKR model (d).

Table 3 | Langmuir, Freundlich, and DKR constants for Cd^{2+} sorption onto HAp_{200} at 298 K

Langmuir adsorption isotherm constants		
q_m (mg g^{-1})	b (L mg^{-1})	R^2
217.4	1.92	0.9892
Freundlich adsorption isotherm constants		
k_f (mg g^{-1})	n	R^2
115.0	3.97	0.9818
DKR adsorption isotherm constants		
X_m (mg g^{-1})	β (mol^2 J^{-2})	R^2
554.4	-1.86×10^{-9}	0.9893

R^2 values exceed 0.98 suggesting a good agreement between the theoretical models and the experimental results. Thus, the maximum sorption capacity q_m obtained with the Langmuir model is 217.4 mg g^{-1}, which is very close to the experimental value of 216.6 mg g^{-1}. Moreover, $1/n$ factor determined from the Freundlich model is in the range of 0.1–1, showing that the adsorption conditions are favourable. E value derived from the DKR model is 16.4 kJ mol^{-1}, suggesting a chemisorption reaction type in which the adsorption is the result of chemical bonds formed between the surface of the adsorbent (HAp_{200}) and the adsorbate (Cd^{2+}). Finally, based on the determined value of q_e, this study showed that a thermal treatment at 200 °C, enhanced the performances of HAp in Cd^{2+} removal from the aqueous medium by more than 100% when compared to the raw material (142.8 mg g^{-1}) (Mobasherpour *et al.* 2011).

Sorption thermodynamics

The thermodynamic data such as Gibbs free energy (ΔG°), enthalpy (ΔH°), and entropy (ΔS°) can be estimated through equilibrium constant changing as a function of the temperature. These parameters are determined using the following equations:

$$\Delta G^\circ = -RT \ln k_d \quad (12)$$

$$\Delta G^\circ = \Delta H^\circ - T\Delta S^\circ \quad (13)$$

$$ln k_d = -\frac{\Delta H^\circ}{RT} + \frac{\Delta S^\circ}{R} \quad (14)$$

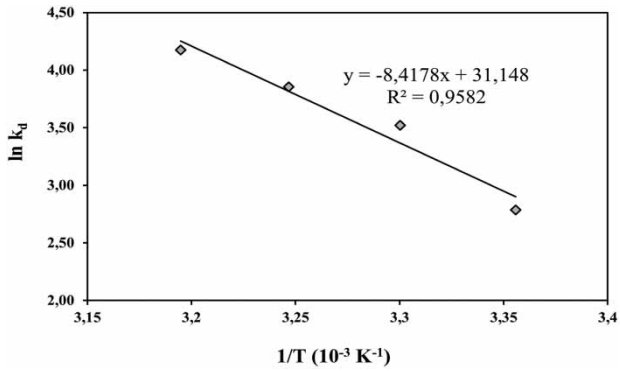

Figure 10 | Plot of ln k_d versus (1/T) for Cd^{2+} adsorption onto HAp_{200}.

In Equation (12), k_d is the distribution ratio ($k_d = q_e/C_e$) and R is the gas constant (8.314 J mol^{-1} K^{-1}). The enthalpy and entropy were determined from the slope and the intercept of the straight-line plot of ln(k_d) versus the reciprocal of absolute temperature (1/T) (Figure 10). These data are summarized in Table 4.

ΔH° is positive and higher than 40 kJ mol^{-1}. Consequently, the adsorption process is endothermic and of chemical nature involving strong attraction forces. Besides, the positive value of ΔS° shows the increase in disorder at the solid–liquid interface.

Sorption mechanisms

Based on a bibliographic survey, ion exchange, surface complexation, and dissolution–precipitation are the main mechanisms involved in the sorption process of cadmium and other heavy metal ions onto hydroxyapatite-based materials (Mobasherpour *et al.* 2011). In this context, SEM and transmission electron microscopy (TEM) observations were carried out to study the morphological variation before and after the interaction with cadmium, on the one hand, and to highlight its higher reactivity toward Cd^{2+} ions compared to HAp_{800}, on the other hand. Also, the sorption mechanisms were investigated by FTIR analyses, a method that has been considered as a kind of direct means to assess the type of interactions between arsenic and bone char (Chen *et al.* 2008).

Table 4 | Thermodynamic data for Cd(II) adsorption on HAp_{200}

		ΔG° (kJ mol^{-1})			
ΔH° (kJ mol^{-1})	ΔS° (J mol^{-1} K^{-1})	298 K	303 K	308 K	313 K
69.98	258.96	−7.18	−8.48	−9.77	−11.07

SEM and TEM observations

According to SEM and TEM micrographs shown in Figure 11, hydroxyapatite particles calcined at 200 and 800 °C have a rod-like shape. However, HAp_{200} looks more heterogeneous with a smaller particle diameter than HAp_{800} which agrees with the measured S_{BET} for HAp_{200} and HAp_{800} determined by the BET method. Moreover, for HAp_{200}, the interactions with cadmium induced a slight increase in particle size and there is no tendency toward the rounded shape.

The EDS analysis illustrated in Figure 12 shows a higher amount of cadmium on the surface of HAp heated at 200 °C than that heated at 800 °C, and consequently, the impact of cadmium sorption on the morphologies of both materials (HAp_{200} and HAp_{800}) was not the same. Hence, in the case of HAp_{800}-Cd, the rounded shape may be explained by the precipitation of leached atoms after the liquid supersaturation. These latter tend to precipitate on the concave and the necks of the particle according to Oswald refinement (Finsy 2004). Accordingly, the origin of these modifications may be related to dissolution/precipitation phenomena. On the other hand, HAp_{200}-Cd shows only an increase of the particle size and a higher amount of cadmium on its surface compared to HAp_{800}-Cd. So, the slight morphological changes may be correlated with the substitution of calcium with cadmium on the surface and/or in the structure, as well as to slow dissolution–precipitation interface reactions.

FTIR analyses

The results of FTIR analyses performed for HAp_{200} before and after Cd(II) adsorption are shown in Figure 13. It can be seen that the PO_4^{3-} absorption bands appearing at 982, 1,030, and 1,071 cm^{-1} and the absorption band of OH^- group at 629 cm^{-1} were significantly shifted to lower frequencies. This phenomenon is related to the distortion of the functional groups induced by the decrease of the lattice volume which is the consequence of the substitution of Ca^{2+}

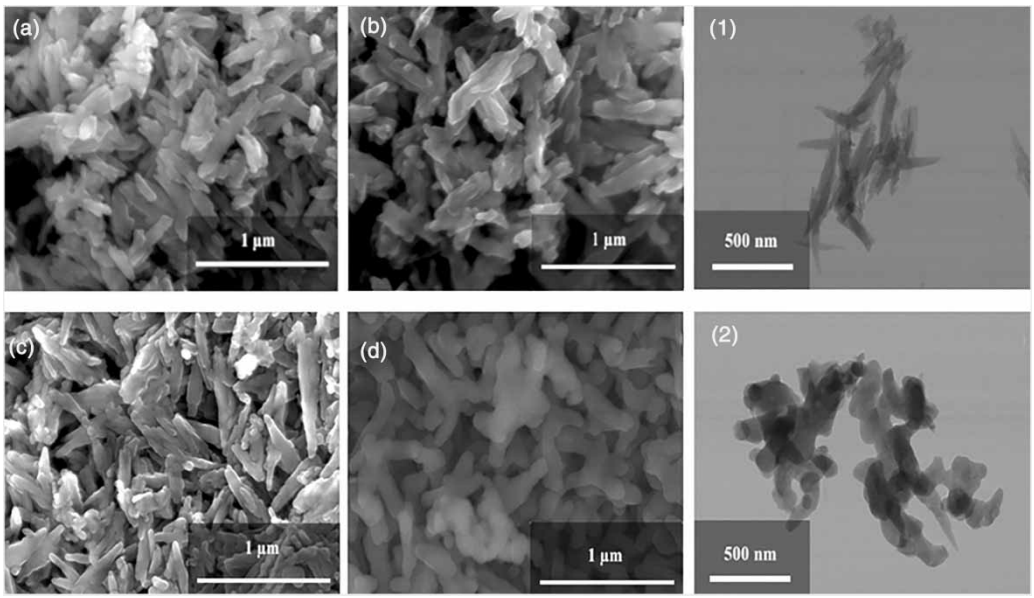

Figure 11 | SEM micrographs relative to HAp_{200} (a), HAp_{200}-Cd (b), HAp_{800} (c), HAp_{800}-Cd (d), and TEM micrographs relative to HAp_{200}-Cd (1) and HAp_{800}-Cd (2).

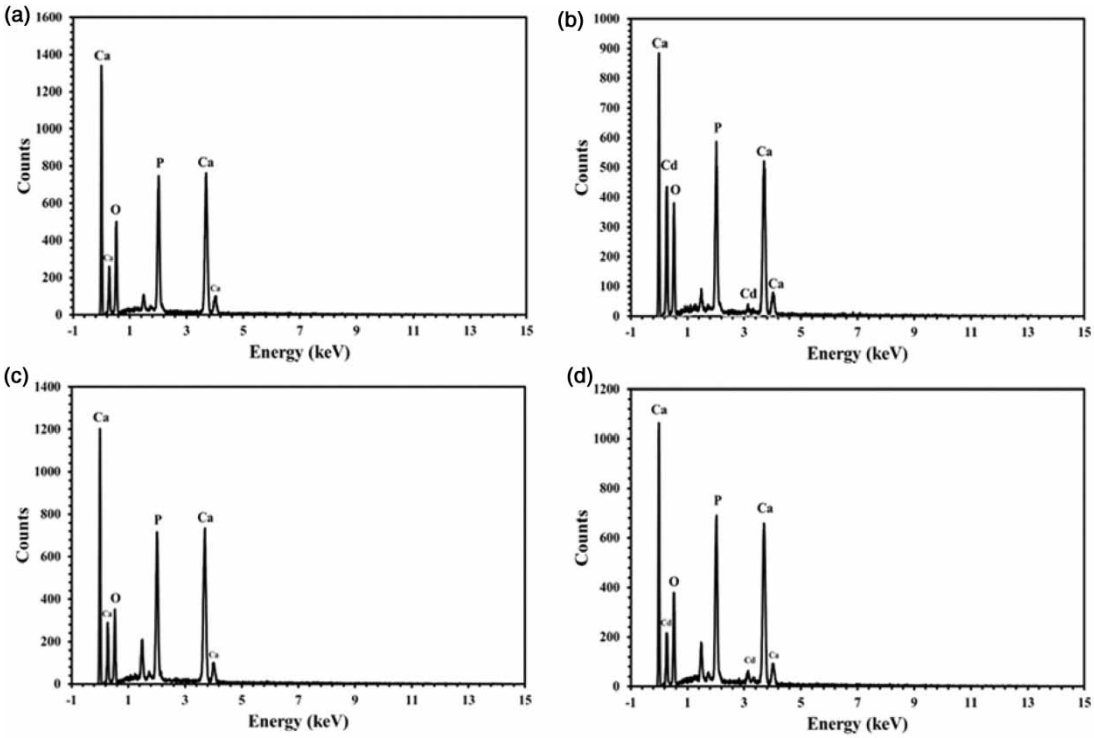

Figure 12 | EDS graphs relative to HAp_{200} (a), HAp_{200}-Cd (b), HAp_{800} (c), and HAp_{800}-Cd (d).

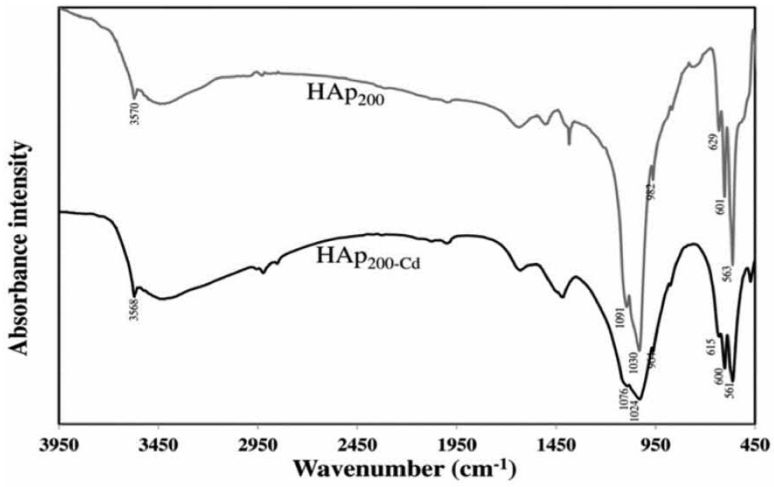

Figure 13 | IR spectrum of the solid residue with a moderate amount of Cd^{2+} uptake ($q_e = 123.6$ mg g^{-1}) compared to that of the starting powder.

by Cd^{2+} (with smaller ionic radius) leading to the formation of a solid solution according to the following scheme:

$$Ca_{10}(PO_4)_6(OH)_{2(s)} + xCd^{2+}_{(aq)} \rightarrow Ca_{(10-x)}Cd_x(PO_4)_6(OH)_{2(s)} + xCa^{2+}_{(aq)}$$

Indeed, Cd^{2+} ions are initially adsorbed onto the HAp_{200} surface by a rapid complexation on ≡POH and $\equiv CaOH_2^+$ sites, then substituted to crystallographic sites of Ca^{2+} atoms. On the other hand, for pH values between 4 and 6, similar studies reported a partial dissolution of $Ca_{10}(PO_4)_6(OH)_2$ followed by the precipitation of Cd-doped apatite with the chemical formula $Ca_{(10-x)}Cd_x(PO_4)_6(OH)_2$ (Mobasherpour *et al.* 2011). Finally, all these mechanisms could occur simultaneously and/or successively as illustrated in Figure 14.

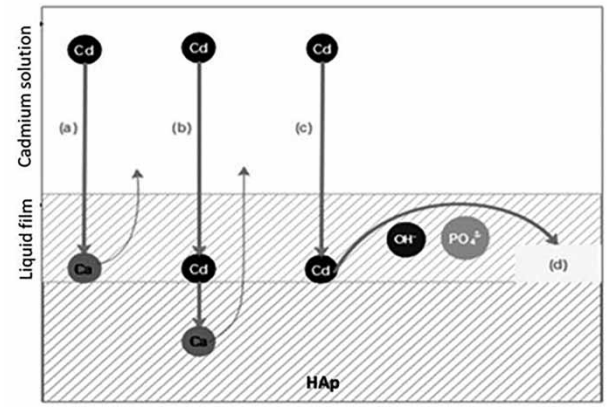

Figure 14 | Mechanisms of Cd removal by HAp_{200}: (a) ion exchange, (b) substitution of calcium in the structure, (c) dissolution/precipitation, and (d) Cd-doped hydroxyapatite.

CONCLUSIONS

This study demonstrates that thermal treatment plays an important role in the capacity of HAp for removing Cd^{2+} ions from contaminated waters. Calcination allowed releasing the residues of the synthesis inserted into the pores of the apatite and consequently enhanced the ability of the material in Cd^{2+} uptake. However, the consumption of energy during this step can be minimized by reducing the heating temperature to 200 °C, while maximizing the Cd^{2+} removal efficiency.

The sorption ability was found to be most affected by some parameters such as the sorbent dosage, the contact time, the initial metal concentration, and the solution temperature. Contrarily, the initial pH of the Cd^{2+} solutions plays only a minor role, especially when shifted from pH 3 to pH 7. Further acidification enhances the adsorption of H_3O^+ protons, turning the surface of the particles less negative, and partially dissolving the HAp particles. These concomitant effects decrease the driving force for the adsorption of Cd^{2+} ions and the uptake capacity observed at pH = 2.

The equilibrium data could reasonably be fitted using Langmuir, Freundlich, and DKR isotherms types. Furthermore, the best kinetic parameters were provided by the pseudo-second-order kinetic model with R^2 values higher than 0.999. The thermodynamic calculations revealed a chemical nature of the adsorption process involving strong attraction forces. The FTIR analysis before and after depollution experiments strongly supported the ion exchange as the predominant mechanism of the sorption process.

FUNDING

This study was supported by the Ministry of Higher Education and Scientific Research of Tunisia, in collaboration with the CICECO-Aveiro Institute of Materials, FCT Ref. UID/CTM/50011/2019, financed by national funds through the FCT/MCTES. Avito H. S. Rebelo acknowledges the Portuguese Foundation for Science and Technology (FCT) for the PhD fellowship grant (SFRH/BD/36101/2007).

DATA AVAILABILITY STATEMENT

All relevant data are included in the paper or its Supplementary Information.

REFERENCES

Adebowale, K. O., Unuabonah, I. E. & Olu-Owolabi, B. I. 2006 The effect of some operating variables on the adsorption of lead and cadmium ions on kaolinite clay. *J. Hazard. Mater.* **134** (1–3), 130–139. https://doi:10.1016/j.jhazmat.2005.10.056.

Chen, Y., Chai, L. & Shu, Y. 2008 Study of arsenic (V) adsorption on bone char from aqueous solution. *J. Hazard. Mater.* **160**, 168–172. https://doi.org/10.1016/j.jhazmat.2008.02.120.

Chen, C., Xun, P., Nishijo, M., Carter, S. & He, K. 2016 Cadmium exposure and risk of prostate cancer: a meta-analysis of cohort and case-control studies among the general and occupational populations. *Sci. Rep.* **6**. https://doi.org/10.1038/srep25814.

Chien, S. H. & Clayton, W. R. 1980 Application of Elovich equation to the kinetics of phosphate release and sorption in soils. *Soil Sci. Soc. Am.* **44**, 265–268. https://doi.org/10.2136/sssaj1980.03615995004400020013x.

Dada, A. O., Olalekan, A. P., Olatunya, A. M. & Dada, O. 2012 Langmuir, Freundlich, Temkin, and Dubinin–Radushkevich isotherms studies of equilibrium sorption of Zn^{2+} unto phosphoric acid modified rice husk. *IOSR J. Appl. Chem.* **3** (1), 38–45. https://doi.org/10.9790/5736-0313845.

Da Rocha, N. C. C., De Campos, R. C., Rossi, A. M., Moreira, E. L., Barbosa, A. D. F. & Moure, G. T. 2002 Cadmium uptake by hydroxyapatite synthesized in different conditions and submitted to thermal treatment. *Environ. Sci. Technol.* **36**, 1630–1635. https://doi.org/10.1021/es0155940.

Dogan, M. & Alkan, M. 2003 Adsorption kinetics of methyl violet onto perlite. *Chemosphere* **50**, 517–528. https://doi.org/10.1016/S0045-6535(02)00629-X.

Elkady, M. F., Mahmoud, M. M. & Abd-El-Rahman, H. M. 2011 Kinetic approach for cadmium sorption using microwave synthesized nano-hydroxyapatite. *Elsevier J. Non-Cryst. Solids* **357**, 1118–1129. https://doi.org/10.1016/j.jnoncrysol.2010.10.021.

Elliot, J. C. 1994 *Studies in Inorganic Chemistry: Structure and Chemistry of the Apatites and Other Calcium Orthophosphates*. Elsevier, Amsterdam.

Finsy, R. 2004 On the critical radius in Ostwald ripening. *Langmuir* **20**, 2975–2976. https://doi.org/10.1021/la035966d.

Harja, M., Buema, G., Bulgariu, L., Bulgariu, D., Sutiman, D. M. & Ciobanu, G. 2015 Removal of cadmium(II) from aqueous solution by adsorption onto modified algae and ash. *Korean J. Chem. Eng.* **32**, 1804–1811. https://doi.org/10.1007/s11814-015-0016-z.

He, M., Shi, H., Zhao, X., Yu, Y. & Qu, B. 2013 Immobilization of Pb and Cd in contaminated soil using nano-crystallite hydroxyapatite. *Procedia Environ. Sci.* **18**, 657–665. https://doi.org/10.1016/j.proenv.2013.04.090.

Ho, Y. 2006 Review of second-order models for adsorption systems. *J. Hazard. Mater.* **136** (3), 681–689. https://doi.org/10.1016/j.jhazmat.2005.12.043.

Idrees, N., Tabassum, B., Abd-Allah, E. F., Hashem, A., Sarah, R. & Hashim, M. 2018 Groundwater contamination with cadmium concentrations in some West U.P. Regions, India. *Saudi J. Biol. Sci.* **25**, 1365–1368. https://doi.org/10.1016/j.sjbs.2018.07.005.

Jebri, S., Khattech, I. & Jemal, M. 2017 Standard enthalpy, entropy and Gibbs free energy of formation of "A" type carbonate phosphocalcium hydroxyapatites. *J. Chem. Thermodyn.* **106**, 84–94. https://doi.org/10.1016/j.jct.2016.10.035.

Jelinek, L. & Kováts, E. 1994 True surface areas from nitrogen adsorption experiments. *Langmuir* **10**, 4225–4231. https://doi.org/10.1021/la00023a051.

Johri, N., Jacquillet, G. & Unwin, R. 2010 Heavy metal poisoning: the effects of cadmium on the kidney. *Biometals* **23**, 783–792. https://doi.org/10.1007/s10534-010-9328-y.

Kheriji, J., Tabassi, D. & Hamrouni, B. 2015 Removal of Cd(II) ions from aqueous solution and industrial effluent using reverse osmosis and nanofiltration membranes. *Water Sci. Technol.* **72**, 1206–1216. https://doi.org/10.2166/wst.2015.326.

Lagergren, S. 1898 About the theory of so called adsorption of soluble substances. *Kungl. Svenska Vetenskapsakad. Handl.* **24** (4), 1–39.

Landi, E., Tampieri, A., Celotti, G. & Sprio, S. 2000 Densification behavior and mechanisms of synthetic hydroxyapatite. *J. Eur. Ceram. Soc.* **20**, 2377–2387. https://doi.org/10.1016/S0955-2219(00)00154-0.

Lin, S. H. & Juang, R. S. 2002 Heavy metal removal from water by sorption using surfactant-modified montmorillonite. *J. Hazard. Mater.* **92**, 315–326. https://doi.org/10.1016/s0304-3894(02)00026-2.

Matusik, J., Bajda, T. & Manecki, M. 2008 Immobilization of aqueous cadmium by addition of phosphates. *J. Hazard. Mater.* **152**, 1332–1339. https://doi.org/10.1016/j.jhazmat.2007.08.010.

McKay, G., Otterburn, M. S. & Aga, J. A. 1985 Fuller's earth and fired clay as adsorbents for dyestuffs. *Water Air Soil Pollut.* **24**, 307–322. https://doi.org/10.1007/BF00161790.

Mobasherpour, I., Salahi, E. & Pazouki, M. 2011 Removal of divalent cadmium cations by means of synthetic nano crystallite hydroxyapatite. *Desalination* **266**, 142–148. https://doi.org/10.1016/j.desal.2010.08.016.

Naeem, M. A., Imran, M., Amjad, M., Abbas, G., Tahir, M., Murtaza, B. & Ahmad, I. 2019 Batch and column scale removal of cadmium from water using raw and acid activated wheat straw biochar. *Water* **11** (7), 1438. https://doi:10.3390/w11071438.

Rajeshkumar, S. & Li, X. 2018 Bioaccumulation of heavy metals in fish species from the Meiliang Bay, Taihu Lake, China. *Toxicol. Rep.* **5**, 288–295. https://doi:10.1016/j.toxrep.2018.01.007.

Stötzel, C., Müller, F. A., Reinert, F., Niederdraenk, F., Barralet, J. E. & Gbureck, U. 2009 Ion adsorption behaviour of hydroxyapatite with different crystallinities. *Colloids Surf. B Biointerfaces* **74**, 91–95. https://doi.org/10.1016/j.colsurfb.2009.06.031.

Wang, D., Guan, X., Huang, F., Li, S., Shen, Y., Chen, J. & Long, H. 2016 Removal of heavy metal ions by biogenic hydroxyapatite: morphology influence and mechanism study. *Russ. J. Phys. Chem. A* **90**, 1557–1562. https://doi.org/10.1134/S0036024416080069.

Weber, T. W. & Chakravoti, R. K. 1974 Pore and solid diffusion models for fixed-bed adsorbers. *AIChE J.* **20**, 228–238. https://doi.org/10.1002/aic.690200204.

Weber, W. J. & Morris, J. C. 1963 Kinetics of adsorption on carbon from solution. *J. Sanit. Eng. Div.* **89**, 31–61.

Wong, C. W., Barford, J. P., Chen, G. & McKay, G. 2014 Kinetics and equilibrium studies for the removal of cadmium ions by ion exchange resin. *J. Environ. Chem. Eng.* **2**, 698–707. https://doi.org/10.1016/j.jece.2013.11.010.

Yingjian, L., Ping, W., Rui, H., Xuxia, L., Peng, W., Jianbin, T., Zihui, C., Zhongjun, D., Jing, W., Qi, J., Shixuan, W., Haituan, L. & Zhixue, L. 2017 Cadmium exposure and osteoporosis: a population-based study and benchmark dose estimation in southern China. *J. Bone Miner. Res.* **32**, 1990–2000. https://doi.org/10.1002/jbmr.3151.

First received 8 July 2020; accepted in revised form 10 September 2020. Available online 17 October 2020